



Enhancing the efficiency and stability of Non-Toxic $\text{RbSn}_{0.5}\text{Ge}_{0.5}\text{I}_3$ -Based perovskite solar cells through optimization



Amina Laouid^{a,b,c,*}, Amine Alaoui Belghiti^a, Krzysztof Wisniewski^{b,c}, Ali Abouais^{a,b}, Mouhaydine Tlemçani^{d,e}, Przemysław Płociennik^{c,f}, Abdelowahed Hajjaji^a, Anna Zawadzka^{b,c}

^a Engineering Science for Energy Lab, National School of Applied Sciences, Chouaib Doukkali University of El Jadida, El Jadida 24000, Morocco

^b Institute of Physics, Faculty of Physics, Astronomy, and Informatics, Nicolaus Copernicus University in Toruń, Grudziadzka 5, PL 87-100 Toruń, Poland

^c Centre for Modern Interdisciplinary Technologies, Nicolaus Copernicus University in Toruń, Wileńska 4, PL 87-100 Toruń, Poland

^d Department of Mechatronics Engineering, School of Science and Technology, Universidade de Évora, Colégio Luís António Verney, Rua Romão Ramalho, N° 59, 7000-671 Évora, Portugal

^e Instrumentation and Control Laboratory, Institute of Earth Sciences, Universidade de Évora, Colégio Luís António Verney, Rua Romão Ramalho, N° 59, 7000-671 Évora, Portugal

^f Institute of Engineering and Technology, Faculty of Physics, Astronomy and Informatics, Nicolaus Copernicus University, Grudziadzka 5, PL 87-100 Toruń, Poland

ARTICLE INFO

Keywords:

SCAPS numerical simulation

SnO_2

Perovskite

MoS_2

Efficiency

ABSTRACT

In the search for alternatives to toxic lead-based perovskite materials, $\text{RbSn}_{0.5}\text{Ge}_{0.5}\text{I}_3$ has emerged as a promising candidate. It offers a nontoxic composition while holding favorable photovoltaic properties. This investigation concentrates exclusively on the utilization of $\text{RbSn}_{0.5}\text{Ge}_{0.5}\text{I}_3$ in perovskite solar cells (PSCs), employing SCAPS_1D simulations to evaluate its performance. Through systematic investigation of a range of parameters such as the thickness of the perovskite layer, the effect of different HOLE TRANSPORT LAYER (HTL) materials, ELECTRON TRANSPORT LAYER (ETL) doping concentration, HTL doping concentration, the defect density of perovskite layer, the defect density of ETL/absorber and absorber/HTL interface, the defect density of ETL and HTLs, series resistance, shunt resistance, various back contacts, and also the temperature on the performance of perovskite solar cells. This investigation aims to optimize the efficiency and stability of $\text{RbSn}_{0.5}\text{Ge}_{0.5}\text{I}_3$ -based PSCs. The optimized device displayed a power conversion efficiency (PCE) of 24.28 %, fill factor (FF) of 78.48 %, and quantum efficiency (QE) of 100 % in the visible range. By revealing the potential of this material in renewable energy applications, the research contributes to the advancement of sustainable photovoltaic technologies. The toxicity of lead-based perovskite materials has been a concern in the development of perovskite solar cells. The investigation for low-toxicity alternatives has led to the exploration of different materials, including Sn -based halide perovskites. The development of stable and efficient perovskite solar cells is required for the advancement of renewable energy technologies, and the research on $\text{RbSn}_{0.5}\text{Ge}_{0.5}\text{I}_3$ -based PSCs contributes to this purpose. Future work will focus on enhancing the scalability of $\text{RbSn}_{0.5}\text{Ge}_{0.5}\text{I}_3$ solar cells, exploring tandem configurations with other photovoltaic materials, and conducting long-term stability assessments in real-world conditions to further validate its commercial viability.

1. Introduction

In recent years, solar cells have been contrived by the increasing global energy need and the demand for durable [1–5], cost-effective, and environmentally friendly energy sources [6–9]. Solar cells, mainly photovoltaic (PV) cells, have occurred as a principal solution to these

challenges, transforming sunlight into electricity employing semiconductor materials [10,11]. The past two decades have seen considerable advancements in solar cell technology, with the most widely used being silicon-based PV cells [12–14]. Nevertheless, the high production costs associated with these cells have conducted researchers to explore alternative materials and structures, such as lead-free perovskite solar

* Corresponding author at: Engineering Science for Energy Lab, National School of Applied Sciences, Chouaib Doukkali University of El Jadida, El Jadida 24000, Morocco.

E-mail address: laouidamina9@gmail.com (A. Laouid).

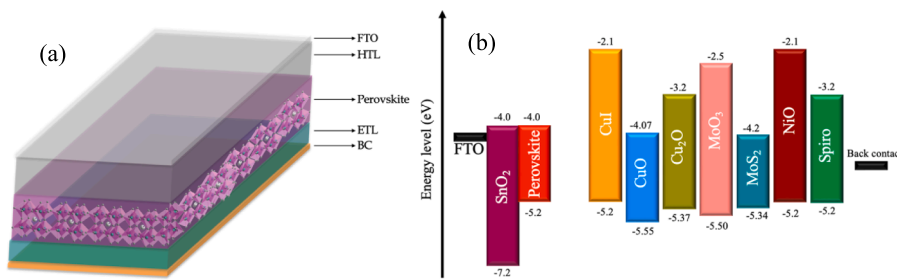


Fig. 1. (a) Device architecture (b) band energy diagram of HTL-based device.

cells (PSCs) [15,16]. Alongside these developments, significant progress has also been made in battery technology, enhancing energy storage solutions for solar power systems [17,18]. Lead-free PSCs present several benefits over traditional silicon-based solar cells, comprising: Higher efficiency due to faster charge carrier diffusion and reduced recombination losses, lower fabrication costs, as they require fewer processing steps and less specialized equipment, environmentally friendly processing, annihilating the use of toxic lead and decreasing waste [19–22]. These advantages have sparked a considerable amount of research and evolution in the field of lead-free PSCs, with various groups investigating different materials and structures to optimize their performance. Some of the key challenges in this area include improving the stability of lead-free PSCs to provide their long-term durability and reliability [23,24], determining the optimal thickness and doping concentrations for the diverse layers of the solar cells to maximize efficiency and minimize production cost and developing adequate encapsulation methods to protect it from environmental degradation and improve their lifetime [25–29].

Among several perovskite compositions, the RbSn_{0.5}Ge_{0.5}I₃ material has garnered considerable attention for its desirable characteristics in executing high-performance photovoltaic devices [30,31]. Despite the promising theoretical predictions for RbSn_{0.5}Ge_{0.5}I₃ as a lead-free alternative in photovoltaic applications, there is currently a lack of extensive experimental data to validate these findings, highlighting the need for further research to explore its practical performance and stability. To exploit the full potential of RbSn_{0.5}Ge_{0.5}I₃ PSCs, a comprehensive understanding of the complex interplay between material properties, device architecture, and external parameters is essential.

The novelty of this work lies in its focused exploration of RbSn_{0.5}Ge_{0.5}I₃ as a lead-free alternative in PSCs, utilizing SCAPS-1D Simulations to systematically analyze a wide range of parameters that influence device performance. Unlike previous studies, this research not only investigates the effects of various etl and htl materials but also delves into the critical role of defect densities and temperature variations on the efficiency and stability of RbSn_{0.5}Ge_{0.5}I₃ PSCs.

The choice of ETL is essential in determining charge carrier dynamics within the perovskite thin film. In this work, we investigate the influence of using SnO₂ as the ETL [32–34], coupled with various HTL materials including Nickel Oxide (NIO) [35], Molybdenum Disulfide (MoS₂) [36], 2,2',7,7'-Tetrakis(N,N-DI-P-Methoxyphenylamine)-9,9'-Spirobi-fluorene (Spiromeotad), Copper(I) Iodide (CuI), Copper(I) Oxide (Cu₂O) and Molybdenum Trioxide MoO₃ [37–41]. Each combination introduces specific charge transport and recombination characteristics, influencing the overall device performance. Furthermore, we delve into the effects of absorber and interface defect densities on the efficiency of RbSn_{0.5}Ge_{0.5}I₃ PSCs. Understanding and minimizing defects are critical for reaching high-performance and stable devices [42,43]. Further, the investigation on the influence of back contact, series resistance (Rs), and shunt resistance (Rsh) on the device performance, was also considered, providing insights into optimizing the electrical characteristics of the solar cells.

Temperature is a critical parameter influencing the efficiency and stability of solar cells [44,45]. Therefore, we examine the temperature

dependence of RbSn_{0.5}Ge_{0.5}I₃ PSCs, elucidating the thermal effects on their photovoltaic performance. The optimized device exhibited a power conversion efficiency of 24.28 %, a fill factor of 78.48 %, and a quantum efficiency of 100 % in the visible range. This indicates that the device is highly efficient in converting solar energy into electrical power. These results combine findings from a comprehensive exploration of these parameters, drawing upon a rich literature base that spans the broader context of perovskite solar cells, thin film technology, and the physics of charge transport in semiconductor devices. By elucidating the intricate relationships between material properties and device parameters, this work contributes to the ongoing efforts to enhance the efficiency and stability of RbSn_{0.5}Ge_{0.5}I₃ PSCs for a sustainable and robust photovoltaic future.

This study employs the SCAPS-1D simulation framework to investigate the efficiency and stability of RbSn_{0.5}Ge_{0.5}I₃-based perovskite solar cells by analyzing various parameters that influence device performance. In particular, the effects of different electron transport layers and hole transport layers, defect interface density, back contact properties, series resistance, and shunt resistance, alongside the impact of defect densities and temperature on photovoltaic performance. Notably, the findings presented in this study contribute significantly to our understanding of optimization strategies for RbSn_{0.5}Ge_{0.5}I₃ pscs, elucidating the intricate relationships between material properties and device architecture. Ultimately, this research underscores the potential impact of advancing lead-free pscs technology in future applications.

2. Modeling and simulation parameters

SCAPS_1D is a one-dimensional simulation software tool employed for simulating the behavior of solar cells [46–48,1,19]. It is a widely utilized simulation tool in the field of solar cell investigation. In the present work, SCAPS_1D has been utilized due to its advantages such as its capability to simulate a broad range of solar cell structures, including homojunctions, heterojunctions, and multijunctions. It simulates also the effects of various parameters on the performance of solar cells, such as defects and doping concentrations, temperature, and illumination intensity. The principle of work of SCAPS_1D is based on Poisson's equation, the electron and hole current densities, and steady-state electron-hole continuity, as it is presented in the following equations [49–52]:

Poisson's equation:

$$-\frac{\partial}{\partial x} \left(-\epsilon(x) \frac{\partial V}{\partial x} \right) = q[p(x) - n(x) + N_D^+(x) - N_A^+(x) + p_t(x) - n_t(x)] \quad (1)$$

$$\text{Continuity equation for electrons : } \frac{\partial n}{\partial t} = \frac{1}{q} \frac{\partial J_n}{\partial x} + G_n - R_n \quad (2)$$

$$\text{Continuity equation for holes : } \frac{\partial p}{\partial t} = \frac{1}{q} \frac{\partial J_p}{\partial x} + G_p - R_p \quad (3)$$

where q is charge, ϵ is dielectric permittivity, V is potential, $p(x)$ is the

Table 1
SCAPS input parameters for the Initial Device configuration.

	SnO ₂	RbSn _{0.5} Ge _{0.5} I ₃	FTO
Eg (eV)	3.2	1.2	3.3
T (nm)	100	—	50
χ (eV)	4	4	4.1
ϵ_r (eV)	9	6.5	9
N_V (cm ⁻³)	$1.8 \cdot 10^{19}$	$1 \cdot 10^{19}$	$2.2 \cdot 10^{18}$
N_e (cm ⁻³)	$2.2 \cdot 10^{18}$	$2 \cdot 10^{18}$	$1.8 \cdot 10^{19}$
μ_e (cm ² /V _s)	20	2	50
μ_p (cm ² /V _s)	10	2	50
N_D (cm ⁻³)	$2 \cdot 10^{18}$	$1 \cdot 10^{15}$	$2 \cdot 10^{18}$
N_A (cm ⁻³)	0	$1 \cdot 10^{15}$	0
v_{Te}	$1 \cdot 10^7$	$1 \cdot 10^7$	$1 \cdot 10^7$
v_{Th}	$1 \cdot 10^7$	$1 \cdot 10^7$	$1 \cdot 10^7$

Table 2
SCAPS input parameters of different HTLs [63,64].

	CuI	CuO	Cu ₂ O	MoS ₂	NiO	Spiro	MoO ₃
T(nm)	500	500	500	500	500	500	500
Eg (eV)	3.1	1.48	2.17	1.23	3.10	2.00	3.00
χ (eV)	2.1	4.07	3.2	4.2	2.1	3.20	2.5
ϵ_r (eV)	6.5	18.10	7.11	4	6.5	3.00	12.50
N_V (cm ⁻³)	1	5.5	1.1	1.8	1.8	2	1.8
	10^{19}	10^{19}	10^{19}	10^{17}	10^{19}	10^{19}	10^{19}
N_e (cm ⁻³)	2.8	2.1	$2 \cdot 10^{17}$	7.5	2.2	1	2.2
	10^{19}	10^{19}		10^{17}	10^{19}	10^{19}	10^{19}
μ_e (cm ² /V _s)	100	100	200	100	100	10^{-4}	25
μ_p (cm ² /V _s)	43.9	0.1	80	150	43.9	10^{-4}	100
N_D (cm ⁻³)	0	0	0	0	0	0	0
N_A (cm ⁻³)	10^{18}	$9 \cdot 10^{16}$	$1 \cdot 10^{18}$	10^{19}	10^{18}	10^{18}	10^{18}
v_{Te}	10^7	10^7	10^7	10^7	10^7	10^7	10^7
v_{Th}	10^7	10^7	10^7	10^7	10^7	10^7	10^7

concentration of free holes, $n(x)$ is the concentration of free electrons, $N_D^+(x)$ is the concentration of ionized donor, $N_A^+(x)$ is a concentration of ionized acceptor, $p_t(x)$ is hole trap density, $n_t(x)$ is electron trap density, J_n is electron current density, J_p is hole current density, G_n is generation rate of electrons, G_p is generation rate of holes, R_n is electron recombination rate and R_p is hole recombination rate.

In Fig. 1(a), a planar perovskite solar cell structure of the n-i-p type is presented. This structure consists of a front contact made of Fluorine-Doped Tin Oxide (FTO) coated Glass, Thin Dioxide (SnO₂) as the Electron Transport Layer (ETL), RbSn_{0.5}Ge_{0.5}I₃ as the light_absorbing material, and various Hole Transport Layers (HTLs) along with Silver (AG) as the back contact.

The initial simulation employs this PSC structure, and the input parameters, detailed in Table 1 and Table 2 [53–57]. The parameters include bandgap (Eg), electron affinity (χ), relative permittivity (ϵ_r), conduction band effective density of states (NC), valence band effective density of states (NV), electron mobility (μ_e), hole mobility (μ_p), donor concentration (ND) and acceptor concentration (NA). [58–62].

The simulation considers a constant illumination of 1000 W.m^{-2} at AM 1.5 G and a temperature of 300 K. To heighten the authenticity, we simulate a modified PSC by introducing interface layers specifically, SnO₂/ RbSn_{0.5}Ge_{0.5}I₃ and RbSn_{0.5}Ge_{0.5}I₃/HTLs. These layers are characterized by a neutral defect density of 10^{13} cm^{-3} and a characteristic energy of 0.6 eV for both interfaces. Additionally, we incorporate defects in all layers with a neutral defect density of 10^{13} cm^{-3} and a characteristic energy of 0.6 eV for both interfaces. The work function of the back contact, Ag, is assumed to be 4.57 eV.

3. Results and discussion

3.1. Effect of absorber layer thickness

The thickness of the absorber layer is a critical parameter that significantly affects the efficiency and characteristics of perovskite solar cells [65–67]. To optimize the performance of these photovoltaic

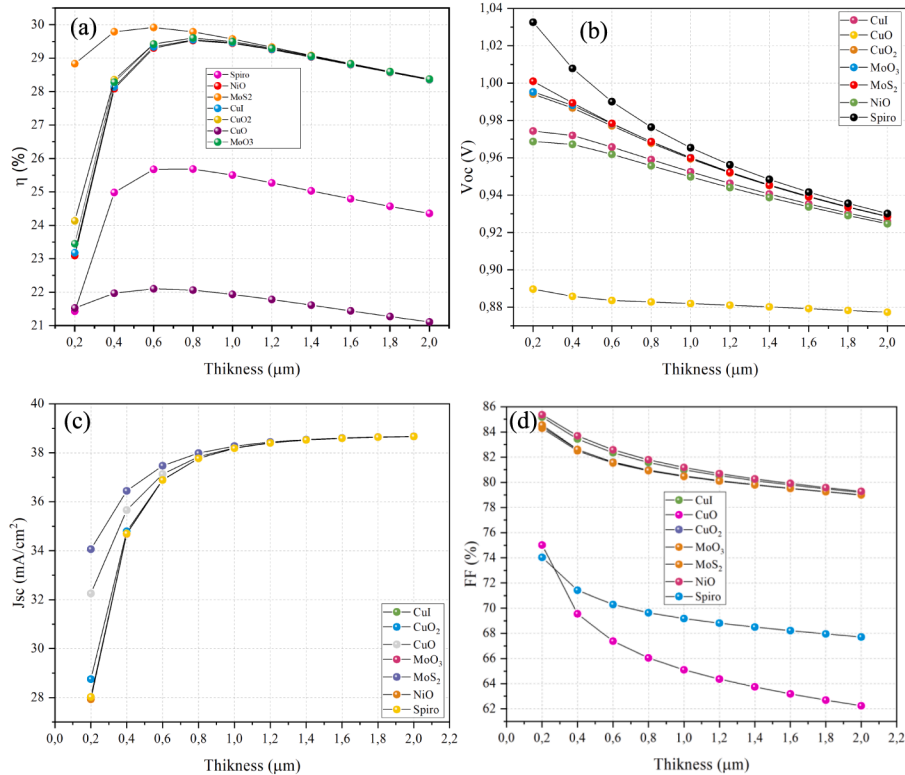


Fig. 2. PCE, V_{oc}, J_{sc}, and FF as a function of the thickness of the absorber.

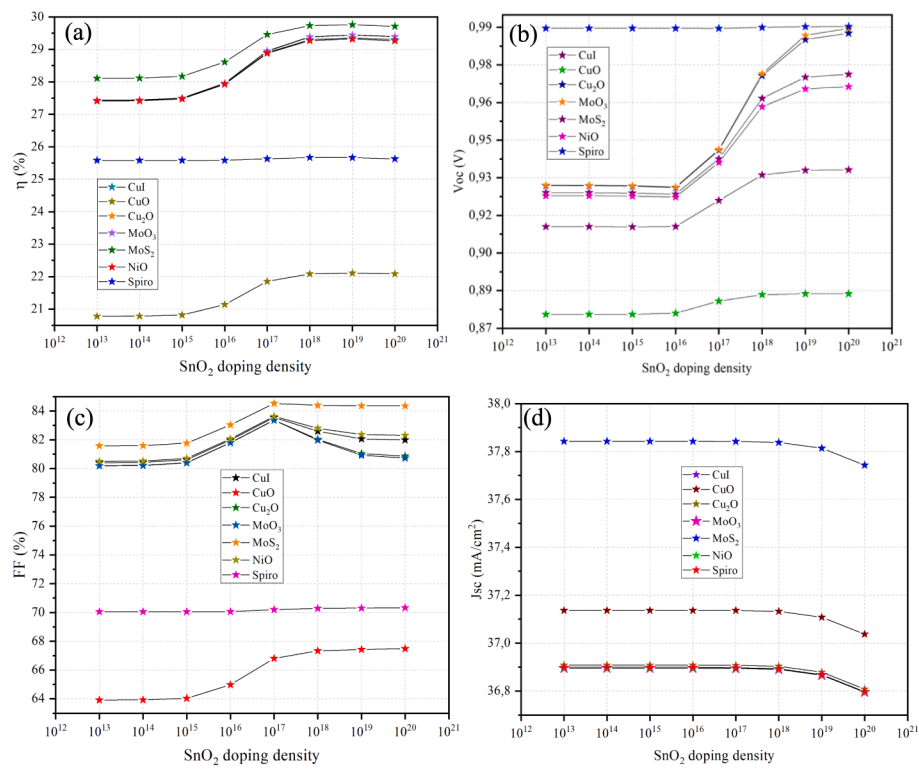


Fig. 3. PCE, V_{OC} , J_{SC} , and FF as a function of the ETL doping density.

devices, an appropriate absorber thickness should be chosen [68]. The thickness of the absorbing layer, in combination with electron transport and hole transport layers, largely determines the performance of the tested device architectures [69]. Increasing the perovskite layer thickness can increase the short-circuit current density of the solar cells [66]. However, the impact of the absorber layer thickness on the overall efficiency of perovskite solar cells is complex and requires meticulous investigation [70]. For that purpose, the thickness of the absorber layer $\text{RbSn}_{0.5}\text{Ge}_{0.5}\text{I}_3$ was investigated between 200 nm to 2000 nm for different HTLs.

Fig. 2 shows the variation in device performance for different absorber thicknesses and different HTLs.

For all the hole transport layers considered, the solar cells exhibit a consistent trend. As the absorber layer thickness increases, the short circuit current and overall efficiency initially experience a rapid ascent, particularly up to 800 nm, due to substantial photon absorption in this range. However, beyond 800 nm, there is a gradual decline in J_{SC} and efficiency with increasing thickness. This can be attributed to the increasing recombination rates associated with the heightened absorber thickness [71,72]. Conversely, the open-circuit voltage and fill factor show a decreasing trend as the absorber thickness increases, also due to the increase in recombination. The MoS₂ has shown the highest parameters for all thickness values, whereas CuI has exhibited lower values. To strike a balance between enhanced photon absorption and mitigated recombination effects, the optimal thickness for the absorber layer is identified as 600 nm for further simulation.

3.2. Effect of ETL doping density

The electron transport layer used in studied perovskite solar cells is SnO_2 . SnO_2 , known as tin dioxide, is a promising candidate for ETL due to its chemical stability and suitable energy levels for electron transport in perovskite solar cells [73]. The doping density of the ETL is critical for modulating charge transport and recombination dynamics, which in turn impacts the overall efficiency of the perovskite solar cells. It

requires careful consideration to optimize the performance and stability of the devices [74,75]. By understanding the nuanced impact of SnO_2 doping density on the photovoltaic characteristics of solar cells, researchers can tailor the properties of the ETL to enhance device efficiency and stability [76]. In this context, the doping density of SnO_2 was investigated in a range of 10^{12} to 10^{18} cm^{-3} for different HTLs as Fig. 3 illustrates.

The research outcomes demonstrate that alterations in SnO_2 doping exerted a notable influence on all device parameters within the investigated structure. Notably, the use of spiroMeOTAD as the hole transport layer resulted in marginal variations in device parameters, while other configurations exhibited distinct responses to SnO_2 doping density. In the case of V_{OC} and efficiency, an incremental enhancement was observed with increasing SnO_2 doping density until reaching 10^{17} cm^{-3} , after which the improvements tapered off. Conversely, J_{SC} exhibited a gradual decline with escalating SnO_2 doping density. The fill factor (FF) data revealed a decreasing trend with diminishing SnO_2 doping density until 10^{17} cm^{-3} , beyond which it began to decline. Notably, when CuO and MoS₂ were employed as the HTL, the parameters continued to improve even after reaching a doping density of 10^{17} cm^{-3} . This behavior of SnO_2 doping density on perovskite solar cell parameters can be attributed to several factors. Firstly, it affects the charge transport and recombination dynamics in the perovskite solar cell, which in turn affects the device efficiency [77]. Further, optimal carrier mobility is achieved at a specific doping density, contributing to the enhancement of the device efficiency [78]. Moreover, the doping density of SnO_2 can affect the charge carrier diffusion length, which is a crucial parameter for the performance of perovskite solar cells. The choice of hole transport layer can also influence the behavior of SnO_2 doping density on device parameters. For example, the use of MoS₂ as the HTL resulted in continuous improvements in device parameters even after reaching a doping density of 10^{17} cm^{-3} .

The value of 10^{17} cm^{-3} , which represents a critical point in the behavior of SnO_2 doping density on perovskite solar cell parameters, will be adopted as a key reference point for the upcoming work. This

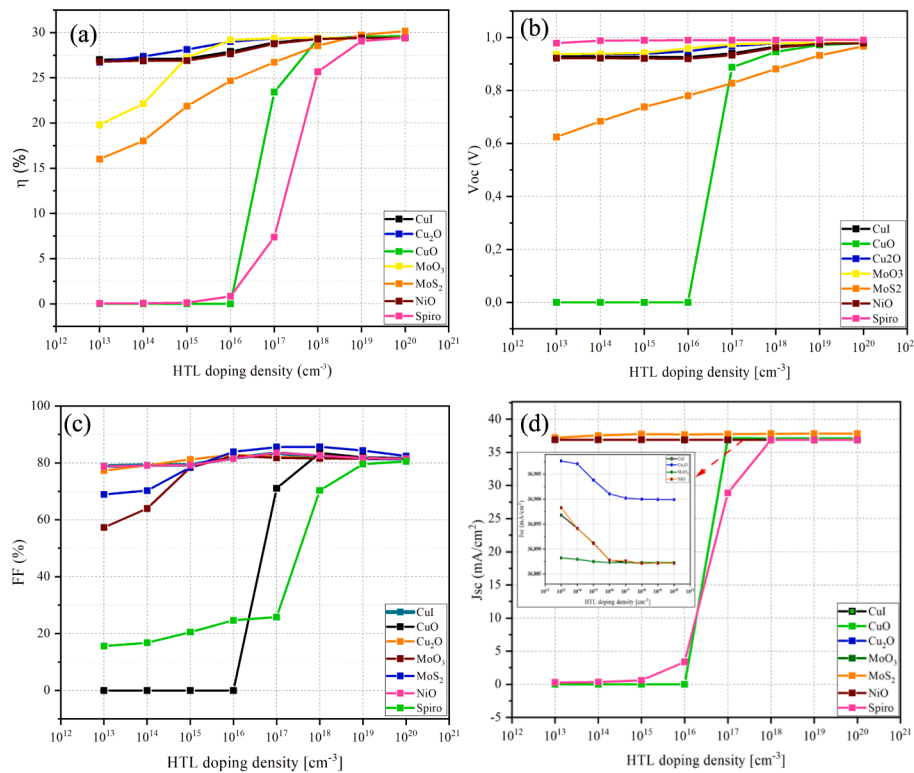


Fig. 4. PCE, V_{OC} , J_{SC} , and FF as a function of the HTL doping density.

value signifies an important threshold at which the influence of SnO₂ doping density on the device parameters undergoes a significant change, as revealed in the study.

3.3. Effect of HTL doping density

The doping density of the hole transport layer is a critical parameter influencing the performance of perovskite solar cells, and its impact varies across different materials [79]. In this investigation, we explore the distinctive effects of HTL doping density on the photovoltaic

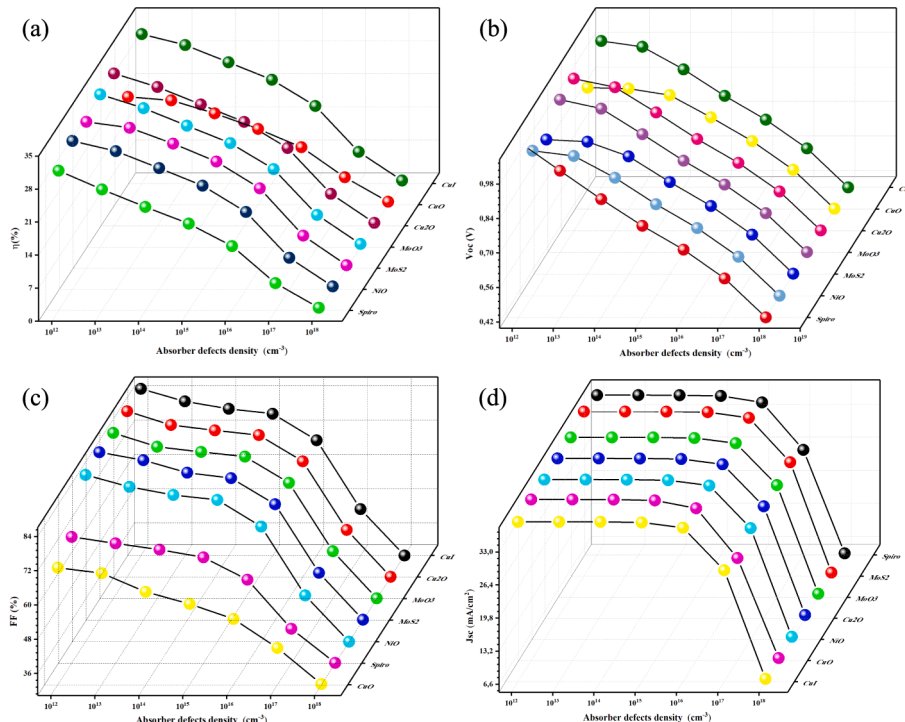
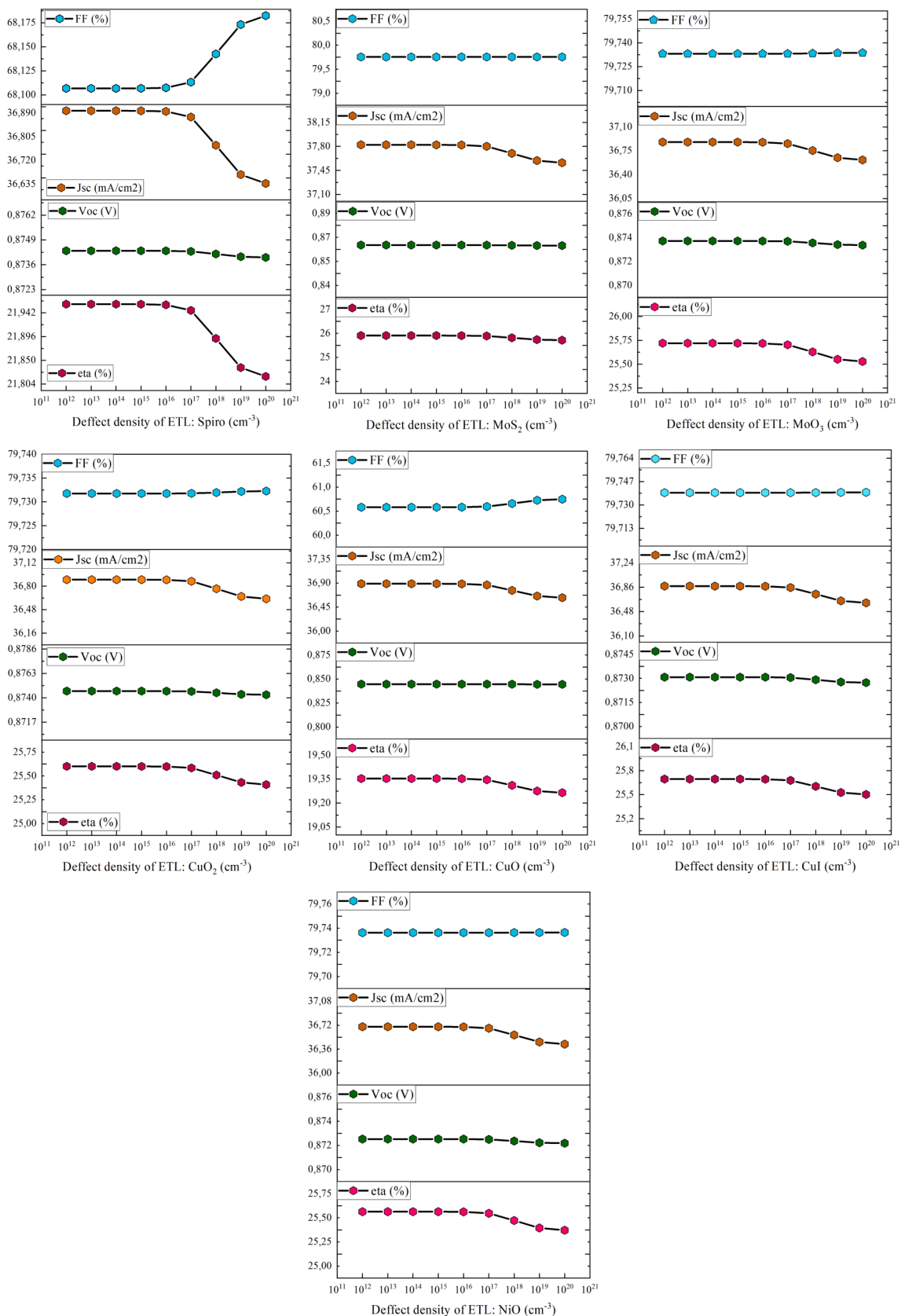


Fig. 5. PCE, V_{OC} , J_{SC} , and FF as a function of the absorber defect density.

Fig. 6. PCE, V_{oc} , J_{sc} , and FF as a function of the ETL defect density.

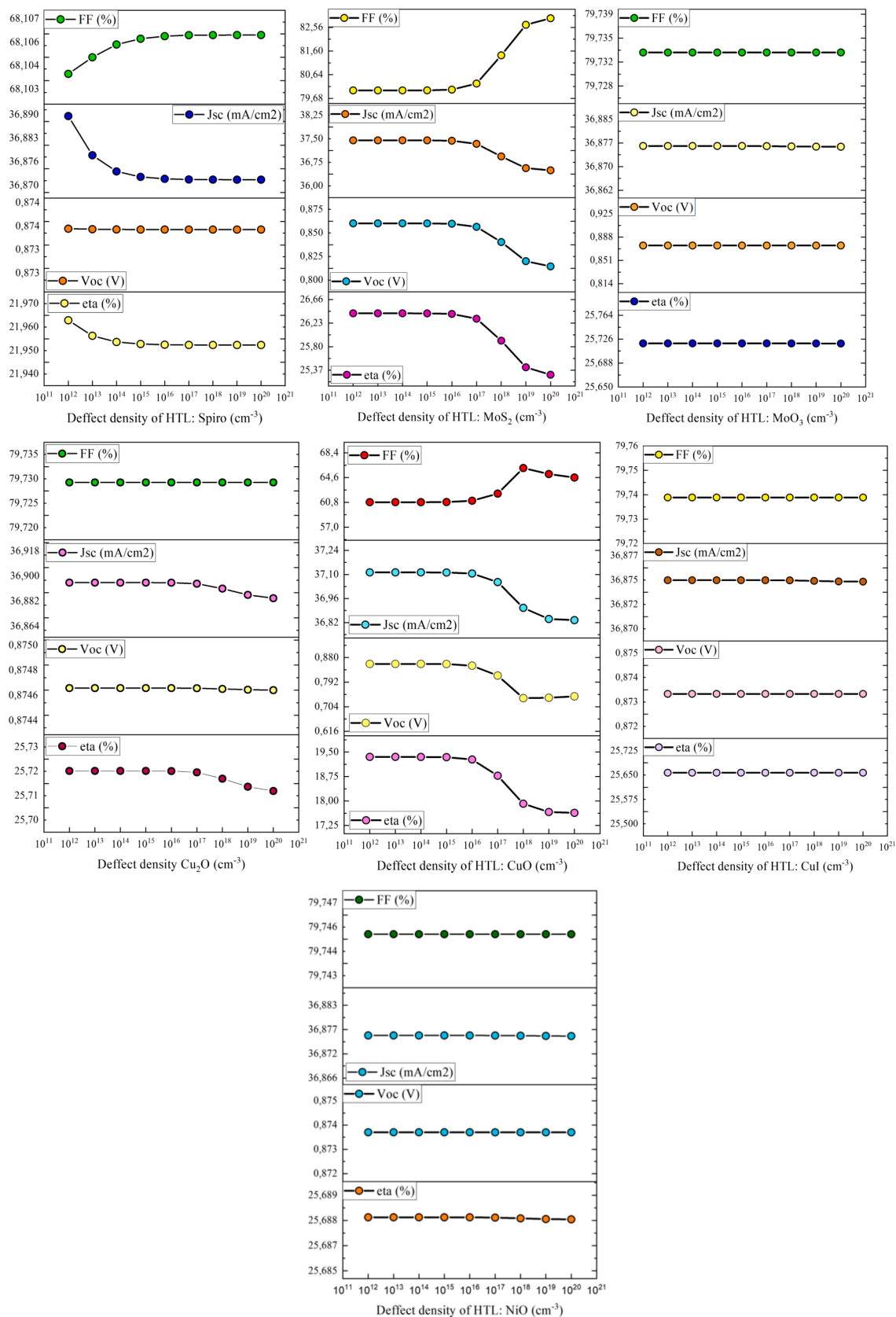


Fig. 7. PCE, Voc, Jsc, and FF as a function of the HTL defect density.

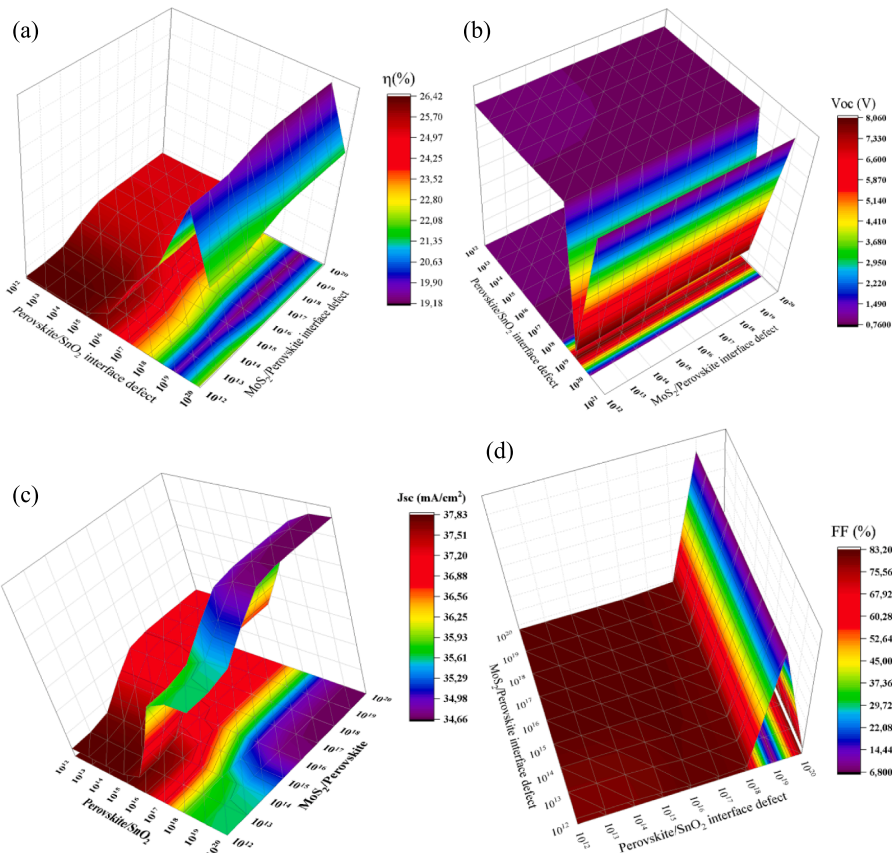


Fig. 8. PCE, V_{OC} , J_{SC} , and FF as a function of the defect interface density.

characteristics of perovskite solar cells utilizing a range of materials, including MoS_2 , spiroMeOTAD, CuI , Cu_2O , MoO_3 , and NiO . Each material represents unique benefits for optimizing charge transport and recombination dynamics. Fig. 4 represents the variation of device performance with HTLs doping density.

The study explored the impact of doping densities ranging from 10^{13} cm^{-3} to 10^{20} cm^{-3} on various hole transport layers in perovskite solar cells. The findings revealed a significant impact of HTL doping density on diverse device parameters, as illustrated in Fig. 4. Both spiroMeOTAD and CuO as HTLs exhibited diminished device parameters at lower doping densities. However, with an increase in density for different HTLs, there was a concurrent rise in device parameters, reaching their respective peak values. This observation highlights the crucial role of HTL doping density in modulating and optimizing the performance of perovskite solar cells across different materials. The increase in HTL doping density can lead to improvements in device parameters such as V_{OC} , J_{SC} , FF, and efficiency due to reduced recombination, improved charge transport, and optimized fill factor [80]. The findings of this study provide valuable insights into the optimization of HTL doping density for improved device efficiency and stability in perovskite solar cells. An optimal doping density of $5 \times 10^{17} \text{ cm}^{-3}$ will be considered for the HTL in the subsequent paragraphs of the article.

3.4. Effect of absorber defect density

The influence of absorber defect density on the performance of perovskite solar cells is an essential aspect that rates detailed investigation. Absorber defects can particularly affect charge transport, recombination processes, and prevailing device efficiency [81]. In this study, we delve into the nuanced effects of varying absorber defect density on key photovoltaic parameters. The absorber defect density was systematically varied in this investigation, ranging from 10^{12} cm^{-3} to

10^{18} cm^{-3} . Fig. 5 depicts the variations in short-circuit current, open-circuit voltage, fill factor, and overall efficiency of the studied structure in response to changes in absorber defect density.

The findings highlight the consistent impact of perovskite defect density on various parameters of the solar cell. It was observed that an increase in absorber defect density led to a uniform decrease in all parameters, including the open circuit voltage, short circuit current, fill factor, and efficiency. This underlines the critical role of perovskite purity in influencing the overall efficiency of the solar cell. The results underscore the importance of maintaining the purity of the perovskite material to achieve optimal performance in perovskite solar cells. The observed decrease in all parameters with an increase in absorber defect density underscores the need for strategies to minimize defects and maintain the purity of the perovskite material in solar cell applications. The optimized value for the perovskite defect density is determined to be 10^{14} cm^{-3} , which will be utilized as the designated value for subsequent calculations.

3.5. Effect of ETL defect density

In the investigation of the effect of Electron Transport Layer Defect Density using SnO_2 as the ETL material, the role of defect density in the performance of perovskite solar cells was examined. Fig. 6 illustrates the impact of Electron Transport Layer defect density on device parameters for various Hole Transport Layers.

The defect density of SnO_2 was systematically varied from 10^{12} cm^{-3} to 10^{20} cm^{-3} , and the findings revealed that no significant changes were observed in the parameters of the device. The influence of defect density on the performance of perovskite solar cells is a subject of extensive research, and the choice of SnO_2 as the ETL material is of particular interest due to its potential impact on device parameters. The systematic variation of defect density provides valuable insights into the behavior

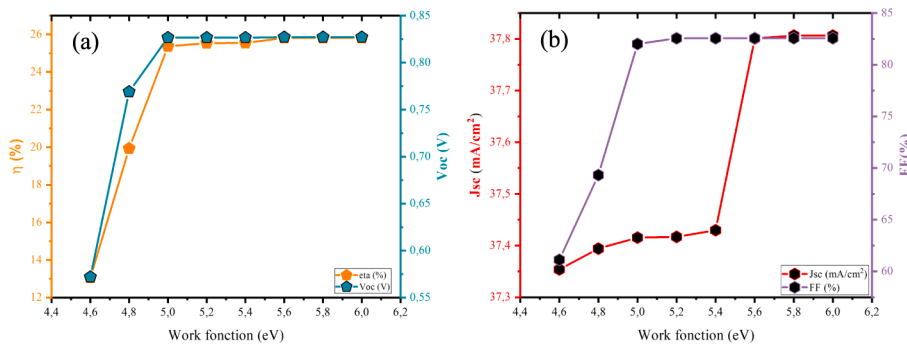


Fig. 9. PCE, V_{oc} , J_{sc} , and FF as a function of the back contact.

of SnO_2 as an ETL material and its influence on the performance of perovskite solar cells. The observed lack of significant changes in device parameters within the studied range of defect densities underscores the need for further investigation and optimization of SnO_2 -based ETLs for improved device efficiency and stability.

3.6. Effect of HTL defect density

The defect density within the Hole Transport Layer plays also an important role in shaping charge transport, recombination processes, and overall device efficiency [82]. In this study, we extensively examine the impacts arising from variations in HTL defect density on crucial photovoltaic parameters. Through a systematic analysis of changes in defect density across a range from 10^{12} cm^{-3} to 10^{18} cm^{-3} for different HTL materials, we aim to unravel the intricate interplay between defects and device performance within the hole transport layer. Our findings indicate a distinctive trend among HTL materials as is presented in Fig. 7. Specifically, for HTLs such as MoO_3 , CuI , and NiO , the defect density appears to have negligible influence on device parameters. On the contrary, in the case of Cu_2O , CuO , spiroMeOTAD, and MoS_2 as HTLs, the device parameters exhibit sensitivity to variations in defect density. Increasing the defect density within these HTLs corresponds to a decrease in device parameters.

This observation underscores the material-specific nature of HTL responses to defect density variations and provides valuable insights for tailoring HTL properties in perovskite solar cells. The choice of HTL material and its defect density can significantly impact the performance of perovskite solar cells. The findings from this study contribute to the understanding of the material-specific responses to defect density variations and guide for optimizing HTL properties for improved device efficiency and stability in perovskite solar cells. Based on the results presented by MoS_2 for a density of 10^{15} cm^{-3} , identified as a hole transport layer, it has been chosen for the subsequent calculations.

3.7. Effect of defect interface density

The examination of the Effect of Defect Interface Density is also a necessary aspect of understanding and optimizing the performance of perovskite solar cells [83]. Specifically, this study focuses on two critical interfaces: $\text{SnO}_2/\text{Perovskite}$ and $\text{Perovskite}/\text{MoS}_2$. The defect interface density at these junctions plays a significant role in influencing charge transport, recombination processes, and overall device efficiency. As Fig. 8 displays, the findings from this study indicate that when the defect interface density at the $\text{SnO}_2/\text{Perovskite}$ and $\text{Perovskite}/\text{MoS}_2$ interfaces exceeds 10^{17} cm^{-3} , there is a noticeable influence on the parameters of the solar cells. When the interface defect ranges from 10^{12} cm^{-3} to 10^{15} cm^{-3} for the $\text{MoS}_2/\text{Perovskite}$ interface and 10^{12} cm^{-3} to 10^{16} cm^{-3} for the $\text{Perovskite}/\text{SnO}_2$ interface, we observed maximum values for J_{sc} at about $37.83 \text{ mA}/\text{cm}^2$ and for efficiency at 26.42 %. Conversely, within the ranges of 10^{18} cm^{-3} to 10^{20} cm^{-3} for $\text{Perovskite}/\text{SnO}_2$ and $5 \text{ to } 10^{16} \text{ cm}^{-3}$ to 10^{20} cm^{-3} , we encountered minimum values for J_{sc} around $34.66 \text{ mA}/\text{cm}^2$ and for efficiency about 19.18 %. The maximum fill factor peaked at approximately 8.06 % for values exceeding $5 \text{ to } 10^{18} \text{ cm}^{-3}$ for $\text{Perovskite}/\text{SnO}_2$, while the minimum of FF was approximately 0.76 % within the same range. V_{oc} measured around 6.8 V for values exceeding $5 \text{ to } 10^{18} \text{ cm}^{-3}$ for $\text{Perovskite}/\text{SnO}_2$, with the maximum reaching 83.20 V for varying values.

The impact of defect density on the performance of perovskite solar cells has been the subject of numerous studies, and the findings from this study contribute to the understanding of the material-specific responses to defect interface density variations. The results provide guidance for optimizing defect interface properties for improved device efficiency and stability in perovskite solar cells. Understanding the mechanisms controlling perovskite solar cell behavior and the impact of defect interface density is crucial for developing strategies to enhance the efficiency and stability of perovskite solar cells.

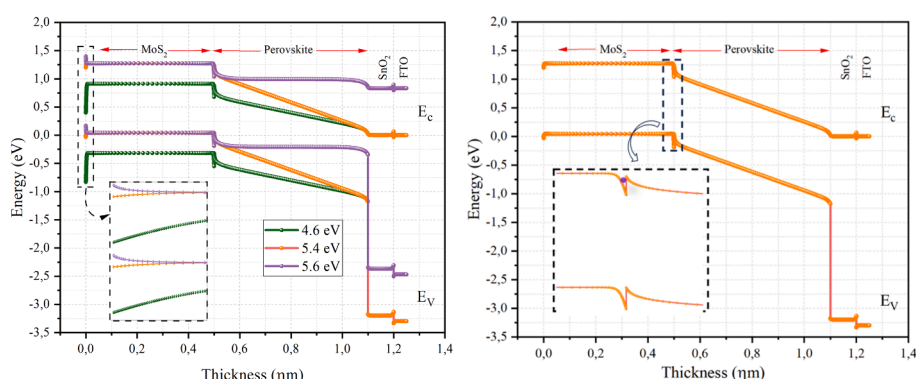


Fig. 10. (a) Energy band diagrams a (b) Spike-like conduction band conformations at the pn-junction.

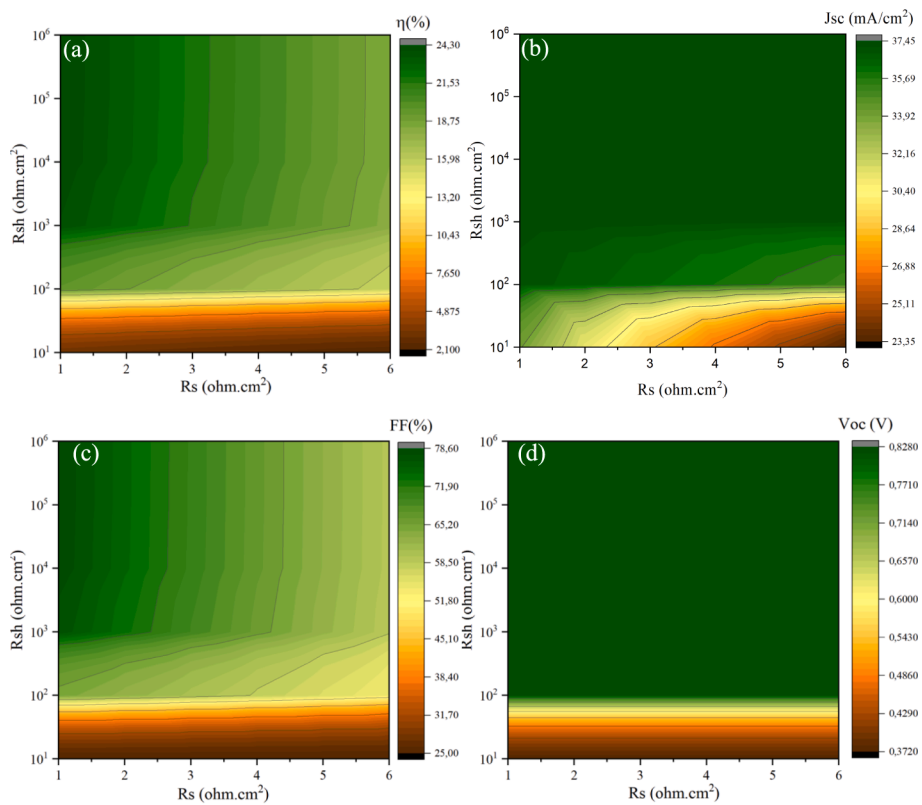


Fig. 11. PCE, V_{oc} , J_{sc} , and FF as functions of series resistance (R_s) and shunt resistance (R_{sh}).

3.8. Effect of back contact

The back contact in a solar cell significantly influences its overall performance [84,85]. By analyzing the impact of different work functions, we gain valuable insights into the nuanced relationship between the back contact and device parameters, which is crucial for optimizing perovskite solar cell designs and maximizing their efficiency.

In this study, the investigation of the impact of varying the work function of the back contact in a solar cell, ranging from 4.6 eV to 6 eV was conducted. As Fig. 9 presents the variation of the back contact work function from 4.6 eV to 5 eV led to a significant improvement in the device parameters. However, beyond 5 eV, the enhancements became more modest, with only a slight increase observed until reaching 6 eV.

The observed phenomenon can be elucidated by the increase in the Schottky barrier for gaps as the work function of the back contact decreases, as depicted by the dashed rectangle in Fig. 10 (a) [85,86]. Consequently, it is recommended that back contacts with a work function exceeding 4.9 eV, such as the base Metals Nickel (NI) and Copper (CU), and the noble metals Gold (AU) and Platinum (PT), are suitable electrodes for Perovskite Solar Cells. Among these, Au has been selected for further investigation.

The band diagram of the FTO/SnO₂/RbSn_{0.5}Ge_{0.5}I₃/MoS₂/Au configuration provides essential insights into energy alignment and charge transport mechanisms within the solar cell. The conduction and valence bands of fto and sno₂ are well-aligned, promoting efficient electron transport from the perovskite layer to the fto electrode. The SnO₂/RbSn_{0.5}Ge_{0.5}I₃ perovskite layer, characterized by a distinct bandgap, enables optimal sunlight absorption and the generation of electron-hole pairs. Fig. 10 (b) represents the spike-like feature at the perovskite/MoS₂ interface in FTO/SnO₂/RbSn_{0.5}Ge_{0.5}I₃/MoS₂/Au structure suggests a favorable energy alignment that facilitates hole transport from the RbSn_{0.5}Ge_{0.5}I₃ perovskite layer to the MoS₂ hole transport layer. This spike configuration can enhance charge extraction, leading to improved efficiency in the solar cell. Conversely, if any

regions exhibit a cliff-like alignment, this could present a potential barrier that impedes hole transport, resulting in increased recombination rates and diminished device performance. Our analysis of the specific energy levels of the conduction and valence bands of both the RbSn_{0.5}Ge_{0.5}I₃ and MoS₂ layers, derived from our SCAPS-1D simulation, reveals significant differences in bandgap energies and electron affinities that contribute to these observed configurations. Referencing relevant studies on similar band alignments further substantiates our discussion and provides a comprehensive understanding of the interface behavior.

3.9. Effect of series resistance (R_s) and shunt resistance (R_{sh})

The investigation of the impact of Series Resistance (R_s) and Shunt Resistance (R_{sh}) on the performance of Perovskite Solar Cells is a fundamental aspect of understanding and optimizing their behavior [87]. In our study, we systematically varied the R_s values from 1 to 6 O.cm² and the R_{sh} values from 100 O.cm² to 106 O.cm². As it is presented in Fig. 11. Our findings revealed a significant influence of these resistance values on the photovoltaic parameters of the PSCs. Specifically, we observed that higher values of R_{sh} , in conjunction with lower values of R_s , led to higher efficiencies. This underscores the critical importance of meticulously optimizing the series and shunt resistances in PSCs to enhance their overall performance. The delicate balance between these resistance parameters plays a pivotal role in determining the efficiency of the solar cells, providing valuable insights for the design and improvement of Perovskite Solar Cell technologies. The origin of series and shunt resistance in solar cells, especially in perovskite solar cells, is attributed to various factors such as the cell structure, material properties, and manufacturing processes. The relationship between series and shunt resistances in solar cells has been studied and estimated using current-voltage measurements. Additionally, the impact of series and shunt resistances on the fill factor and overall power losses in solar cells has been extensively discussed in the literature. These findings align

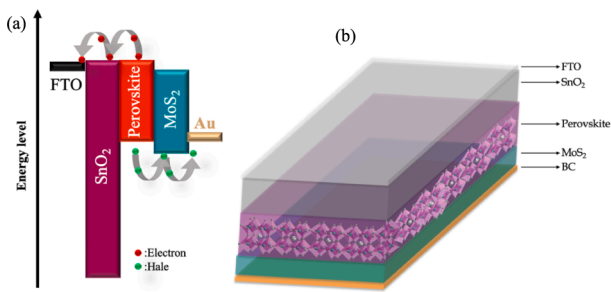


Fig. 12. (a) Device architecture (b) band energy diagram of the optimized structure.

Table 3
Input parameters of used materials.

	FTO	SnO ₂	RbSn _{0.5} Ge _{0.5} I ₃	MoS ₂
E _g (eV)	3.3	3.2	1.2	1.23
T (nm)	50	100	—	500
χ (eV)	4.1	4	4	4.2
ϵ_r (eV)	9	9	6.5	4
N_V (cm ⁻³)	$2.2 \cdot 10^{18}$	$1.8 \cdot 10^{19}$	$1 \cdot 10^{19}$	$1.8 \cdot 10^{17}$
N_c (cm ⁻³)	$1.8 \cdot 10^{19}$	$2.2 \cdot 10^{18}$	$2 \cdot 10^{18}$	$7.5 \cdot 10^{17}$
μ_e (cm ² /V _s)	50	20	2	100
μ_p (cm ² /V _s)	50	20	2	150
N_D (cm ⁻³)	$2 \cdot 10^{18}$	$1 \cdot 10^{17}$	$1 \cdot 10^{15}$	0
N_A (cm ⁻³)	0	0	$1 \cdot 10^{15}$	$5 \cdot 10^{17}$
v_{Te}	$1 \cdot 10^7$	$1 \cdot 10^7$	$1 \cdot 10^7$	10^7
v_{Th}	$1 \cdot 10^7$	$1 \cdot 10^7$	$1 \cdot 10^7$	10^7

Table 4
Defects interfaces.

Interfaces	Defects (cm ⁻³)
MoS ₂ /Perovskite	10^{14}
Perovskite/SnO ₂	10^{16}

with our observations and contribute to the comprehensive understanding of the role of series and shunt resistances in the performance of Perovskite Solar Cells.

3.10. Optimized device performance

The optimized structure is FTO/SnO₂/RbSn_{0.5}Ge_{0.5}I₃/MoS₂/Au and its parameters are presented in Fig. 12 and Tables 3 and 4 respectively.

The J_V and Quantum Efficiency (QE) curves are illustrated in Fig. 13. The QE curve exhibits the maximum conversion of photons to electrons across the entire spectrum (Fig. 13 a). Notably, the QE reaches

its peak value between 380 and 950 nm before dropping to zero at 1050 nm. Ultimately, the best Perovskite Solar Cell device parameters for our configuration, considering the optimized ETL, HTL, absorber layer, series resistance (R_s = 1 Ohm.cm²), and shunt resistance (R_{sh} = 1 10^6 Ohm.cm²), are Voc = 0.82 V, J_{sc} = 37.42 mA/cm², FF=78.48 %, and η = 27.18 %, respectively. The investigation of the effect of Series Resistance and Shunt Resistance on the performance of Perovskite Solar Cells is a critical aspect of understanding and optimizing their behavior.

3.11. Temperature effect on PSC device performance

To gain a deeper understanding of the impact of environmental conditions on the performance of our optimized structure, we conducted calculations to assess the Perovskite Solar Cell parameters across various temperatures [88]. Fig. 14 presents the J_V curve of our device recorded at different operational temperatures.

The analysis revealed that Voc, FF, and η exhibited gradual decreases from 0.82 to 0.63 V, 78.48 % to 69.57 %, and 24.28 % to 16.60 %, respectively, as the temperature increased from 300 K to 420 K, as illustrated in Fig. 15. This decline in PSC parameters can be attributed to the heightened recombination rate and saturation current associated with temperature elevation. However, the J_{sc} value showed a notable increase from 37.42 to 37.50 mA/cm², which can be linked to increased coulombic scattering, which negatively impacts both carrier mobility and lifetime. As temperature rises, the thermal energy of charge carriers increases, leading to more frequent collisions with lattice ions, thereby reducing their effective mobility. This heightened scattering results in fewer charge carriers contributing to the current flow. Additionally, higher temperatures can increase carrier recombination rates, shortening the lifetime of charge carriers and further diminishing the J_{SC}. The specific materials used, such as SnO₂ and the perovskite layer RbSn_{0.5}Ge_{0.5}I₃, may exhibit varying responses to temperature changes, influencing their conductivity and overall performance. In essence, the overall performance of the device experienced degradation at higher temperatures. The stability of PSCs at high temperatures has been a challenge, and researchers have been exploring ways to minimize PSC degradation at high temperatures. The fill factor of PSCs is considerably lower than that of conventional solar cells, and it is governed by recombination and series resistance at the maximum power point (MPP), in the absence of shunts.

As Table 5 presents, RbSn_{0.5}Ge_{0.5}I₃ solar cells are distinguished within the photovoltaic landscape due to their remarkable combination of high efficiency—reaching up to 24 %, which is on par with lead-based perovskites—and improved stability. These cells circumvent the toxicity and environmental issues linked to lead, presenting a viable alternative to tin-based perovskites, which often face challenges with lower efficiency and stability. Although RbSn_{0.5}Ge_{0.5}I₃ cells are still in the research phase and not yet commercially available, their promising characteristics position them as frontrunners for future solar

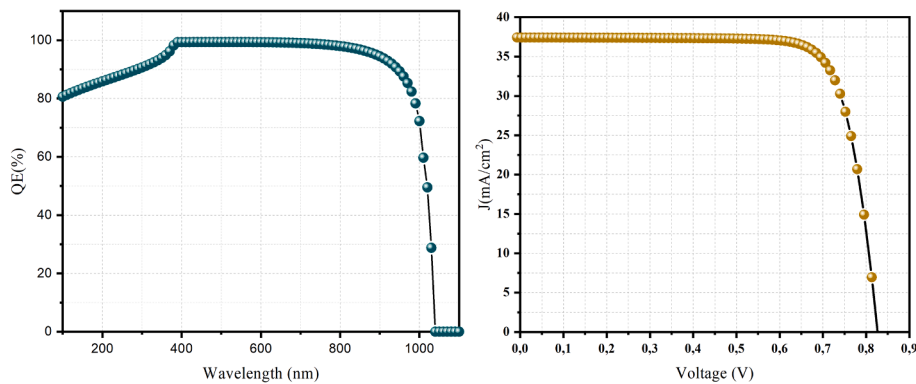


Fig. 13. J_V characteristics and QE curves for the optimized device.

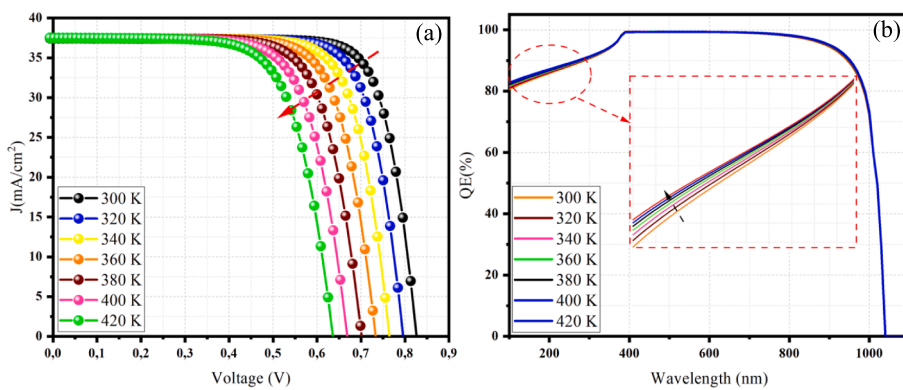


Fig. 14. J-V characteristic QE curves for different operational temperatures.

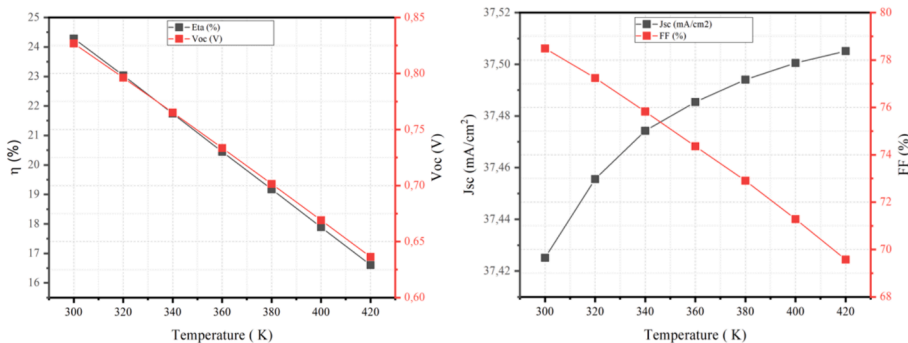


Fig. 15. Temperature effect on PSC device performance.

Table 5
Limitations of Other Competitive Technique.

TECHNIQUE	ADVANTAGES	LIMITATIONS
LEAD-BASED PEROVSKITES [89]	HIGH EFFICIENCY (UP TO 26 %)	TOXICITY OF LEAD, STABILITY ISSUES, ENVIRONMENTAL CONCERN
TIN-BASED PEROVSKITES [90]	LEAD-FREE, LOWER TOXICITY	LOWER EFFICIENCY (TYPICALLY <15 %), STABILITY CHALLENGES
ORGANIC PHOTOVOLTAICS [91]	FLEXIBLE, LIGHTWEIGHT	LOWER EFFICIENCY (TYPICALLY <10 %), LIMITED STABILITY
DYE-SENSITIZED SOLAR CELLS [91]	SIMPLE FABRICATION, ECONOMICALLY ADVANTAGEOUS	LOWER EFFICIENCY (TYPICALLY <12 %), LIMITED LIFETIME
RbSn _{0.5} Ge _{0.5} I ₃ SOLAR CELLS [THIS WORK]	HIGH EFFICIENCY (UP TO 24 %), STABILITY	STILL UNDER RESEARCH, LESS COMMERCIAL AVAILABILITY

technologies.

4. Conclusion

The research presented in this study demonstrates a comprehensive investigation into the performance enhancement of RbSn_{0.5}Ge_{0.5}I₃-based perovskite solar cells (PSCs) through SCAPS-1D simulations. By systematically exploring the impact of various parameters such as the choice of hole transport layer and electron transport layer materials, their thicknesses, and the doping concentrations of the different layers, the study has contributed to the optimization of the efficiency and stability of lead-free PSCs. The findings demonstrate that the optimized device exhibited a high-power conversion efficiency (PCE) of 24.28 %, a fill factor (FF) of 78.48 %, and a quantum efficiency (QE) of 100 % in the

visible range, indicating its potential for converting solar energy into electrical power with high efficiency and stability. The significance of this research lies in its contribution to the development of sustainable and robust photovoltaic technologies. By addressing the challenges associated with lead-based perovskite materials, such as their toxicity and the stability of PSCs at high temperatures, the study has advanced the exploration of low-toxicity alternatives and provided insights into minimizing PSC degradation. Furthermore, the investigation of the intricate relationships between material properties and device parameters has broader implications for the advancement of renewable energy technologies. In conclusion, the findings of this study not only underscore the potential of RbSn_{0.5}Ge_{0.5}I₃ as a promising candidate for lead-free PSCs but also provide valuable insights into the optimization of PSC performance. The research contributes to the ongoing efforts to enhance the efficiency and stability of lead-free PSCs, thereby supporting the transition towards a more sustainable and environmentally friendly energy landscape. The choice of HTL and ETL materials, their thicknesses, and the doping concentrations of the different layers have been shown to significantly impact the performance of the lead-free PSCs, highlighting the importance of these factors in the development of high-efficiency and stable solar cell technologies.

Formatting of funding sources

The research was carried out as part of the IDUB project – emerging research fields: “Material Science and Technology”.

CRediT authorship contribution statement

Amina Laouid: Writing – original draft, Software, Investigation, Funding acquisition, Formal analysis, Data curation. **Amine Alaoui Belghiti:** Writing – review & editing, Validation, Supervision. **Krzysztof Wisniewski:** Writing – review & editing, Formal analysis, Data curation.

Ali Abouais: Software, Resources, Investigation. **Mouhaydine Tlemçani:** Investigation, Funding acquisition, Formal analysis. **Przemysław Płociennik:** Validation, Software, Investigation, Data curation. **Abdelouahed Hajjaji:** Writing – review & editing, Validation, Supervision. **Anna Zawadzka:** Writing – review & editing, Validation, Supervision, Methodology.

Declaration of competing interest

The authors declare that they have no known competing financial interests or personal relationships that could have appeared to influence the work reported in this paper.

Data availability

Data will be made available on request.

Acknowledgment

All authors gratefully acknowledge the SCAPS simulation software provided by Mr. Marc Burgelman.

References

- [1] M.K. Hossain, G.F.I. Toki, A. Kuddus, M.K.A. Mohammed, R. Pandey, J. Madan, et al., Optimization of the architecture of lead-free CsSnCl₃-perovskite solar cells for enhancement of efficiency: a combination of SCAPS-1D and wxAMPS study, Mater. Chem. Phys. 308 (2023) 128281, <https://doi.org/10.1016/j.matchemphys.2023.128281>.
- [2] M.F. Rahman, M.M. Alam Moon, M.K. Hossain, M.H. Ali, M.D. Haque, A. Kuddus, et al., Concurrent investigation of antimony chalcogenide (Sb₂Se₃ and Sb₂S₃)-based solar cells with a potential WS₂ electron transport layer, Heliyon 8 (2022) e12034.
- [3] M.H. Ali, M.A. Al Mamun, M.D. Haque, M.F. Rahman, M.K. Hossain, A.Z. Md. Touhidul Islam, Performance enhancement of an MoS₂-based heterojunction solar cell with an In₂Te₃ back surface field: a numerical simulation approach, ACS Omega 8 (2023) 7017–7029, <https://doi.org/10.1021/acsomega.2c07846>.
- [4] A. Laouid, A. Alaoui Belghiti, K. Wisniewski, J. Strzelecki, A. Karakas, A. Gozutok, et al., Optical and morphological properties of DCM thin films co-doped of Znq2 by PVD: theoretical and experimental investigations, Vacuum 222 (2024) 112997, <https://doi.org/10.1016/j.vacuum.2024.112997>.
- [5] A. Laouid, A.A. Belghiti, K. Wisniewski, A. Hajjaji, B. Sahraoui, A. Zawadzka, Generation of red light with intense photoluminescence assisted by Forster resonance energy transfer from Znq2 and DCM thin films, Environ. Sci. Pollut. Res. (2022) 1–20, <https://doi.org/10.1007/s11356-022-23217-z>.
- [6] H. Bencherif, H.M. Khalid, Design and numerical investigation of efficient (FAPbI₃)_{1-x}(CsSnI₃)_x perovskite solar cell with optimized performances, Sol. Energy 248 (2022) 137–148, <https://doi.org/10.1016/j.solener.2022.11.012>.
- [7] M. Mammari, L. Dehimi, H. Bencherif, F. Pezzimenti, Paths towards high perovskite solar cells stability using machine learning techniques, Sol. Energy 249 (2023) 651–660, <https://doi.org/10.1016/j.solener.2022.12.002>.
- [8] A. Zawadzka, A. Marjanowska, A. Laouid, K. Wisniewski, Y. El Kouari, P. Plociennik. Low-temperature influence on the properties and efficiency of thin-film perovskite solar cells fabricated by the PVco-D technique 2024. Doi: 10.1016/j.solmat.2024.112993.
- [9] A. Laouid, A. Alaoui Belghiti, K. Wisniewski, M. Boumhamdi, J. Strzelecki, P. Plociennik, et al., A study of morphological, optical, and photoluminescence properties of ZnS thin films doped Mn and ca, Mater. Chem. Phys. (2024) 129270, <https://doi.org/10.1016/j.matchemphys.2024.129270>.
- [10] C. Zhu, Optimizing and using AI to study of the cross-section of finned tubes for nanofluid-conveying in solar panel cooling with phase change materials, Eng. Anal. Bound. Elem. 157 (2023) 71–81, <https://doi.org/10.1016/j.enganabound.2023.08.018>.
- [11] C. Zhu, M. Wang, M. Guo, J. Deng, Q. Du, W. Wei, et al., Optimizing solar-driven multi-generation systems: A cascade heat recovery approach for power, cooling, and freshwater production, Appl. Therm. Eng. 240 (2024) 122214, <https://doi.org/10.1016/j.applthermaleng.2023.122214>.
- [12] J. Pastuszak, P. Węgierek, Photovoltaic Cell Generations and Current Research Directions for Their Development, Materials 15 (2022) 5542, <https://doi.org/10.3390/ma15165542>.
- [13] D. Yan, A. Cuevas, J. Stuckelberger, E.-C. Wang, S.P. Phang, T.C. Kho, et al., Silicon solar cells with passivating contacts: Classification and performance, Prog. Photovolt. Res. Appl. 31 (2023) 310–326, <https://doi.org/10.1002/pip.3574>.
- [14] J. Ibarra Michel, J. Dréon, M. Boccard, J. Bullock, B. Macco, Carrier-selective contacts using metal compounds for crystalline silicon solar cells, Prog. Photovolt. Res. Appl. 31 (2023) 380–413, <https://doi.org/10.1002/pip.3552>.
- [15] M. Chen, M.-G. Ju, H.F. Garces, A.D. Carl, L.K. Ono, Z. Hawash, et al., Highly stable and efficient all-inorganic lead-free perovskite solar cells with native-oxide passivation, Nat. Commun. 10 (2019) 16, <https://doi.org/10.1038/s41467-018-07951-y>.
- [16] T. Wu, X. Liu, X. Luo, X. Lin, D. Cui, Y. Wang, et al., Lead-free tin perovskite solar cells, Joule 5 (2021) 863–886, <https://doi.org/10.1016/j.joule.2021.03.001>.
- [17] X. Zhang, Y. Tang, F. Zhang, C.-S. Lee, A Novel Aluminum-Graphite Dual-Ion Battery, Adv. Energy Mater. 6 (2016) 1502588, <https://doi.org/10.1002/aenm.201502588>.
- [18] M. Wang, C. Jiang, S. Zhang, X. Song, Y. Tang, H.-M. Cheng, Reversible calcium alloying enables a practical room-temperature rechargeable calcium-ion battery with a high discharge voltage, Nat. Chem. 10 (2018) 667–672, <https://doi.org/10.1038/s41557-018-0045-4>.
- [19] A.E. Magdalin, P.D. Nixon, E. Jayaseelan, M. Sivakumar, S.K.N. Devi, M.S. P. Subathra, et al., Development of lead-free perovskite solar cells: opportunities, challenges, and future technologies, Results Eng. 20 (2023) 101438, <https://doi.org/10.1016/j.rineng.2023.101438>.
- [20] M. Wang, W. Wang, B. Ma, W. Shen, L. Liu, K. Cao, et al., Lead-free perovskite materials for solar cells, Nano-Micro Lett. 13 (2021) 62, <https://doi.org/10.1007/s40820-020-00578-z>.
- [21] Y. Miao, M. Ren, Y. Chen, H. Wang, H. Chen, X. Liu, et al., Green solvent enabled scalable processing of perovskite solar cells with high efficiency, Nat. Sustain. 6 (2023) 1465–1473, <https://doi.org/10.1038/s41893-023-01196-4>.
- [22] X. Wu, D. Zhang, X. Wang, X. Jiang, B. Liu, B. Li, et al., Eco-friendly perovskite solar cells: from materials design to device processing and recycling, EcoMat 5 (2023) e12352.
- [23] T.J. Macdonald, L. Lanzetta, X. Liang, D. Ding, S.A. Haque, Engineering stable lead-free tin halide perovskite solar cells: lessons from materials chemistry, Adv. Mater. 35 (2023) 2206684, <https://doi.org/10.1002/adma.202206684>.
- [24] R.S. Bobba, N. Ghimire, M.B. Faheem, S. Mabrouk, A. Baniya, N. Narwal, et al., Thioacetamide-assisted crystallization of lead-free perovskite solar cells for improved efficiency and stability, Sol. RRL 7 (2023) 2300191, <https://doi.org/10.1002/solr.202300191>.
- [25] P.A.M. Mercy, K.S.J. Wilson, Design of an innovative high-performance lead-free and eco-friendly perovskite solar cell, Appl. Nanosci. 13 (2023) 3289–3300, <https://doi.org/10.1007/s13204-022-02745-7>.
- [26] K. Ahmad, M. Quasim Khan, A. Alsulmi, H. Kim, Numerical simulation and experimental study of methyl ammonium bismuth iodide absorber layer based lead free perovskite solar cells, Chem – Eur J 29 (2023) e202300513.
- [27] S. Mushtaq, S. Tahir, A. Ashfaq, R. Sebastian Bonilla, M. Haneef, R. Saeed, et al., Performance optimization of lead-free MASnBr 3 based perovskite solar cells by SCAPS-1D device simulation, Sol. Energy 249 (2023) 401–413, <https://doi.org/10.1016/j.solener.2022.11.050>.
- [28] O.M. Durodola, C. Ugwu, E. Danladi, Highly efficient lead-free perovskite solar cell based on magnesium-doped copper delafossite hole transport layer: a SCAPS-1D framework prospect, Emergent Mater. 6 (2023) 1665–1684, <https://doi.org/10.1007/s42247-023-00542-8>.
- [29] R.S. Almufarrij, A. Ashfaq, S. Tahir, R.S. Alqurashi, A.H. Ragab, D.E. El-Refaey, et al., Improving performance and recombination losses in lead free formamidinium tin based perovskite solar cells, Mater. Chem. Phys. 307 (2023) 128150, <https://doi.org/10.1016/j.matchemphys.2023.128150>.
- [30] X.-Z. Deng, Q.-Q. Zhao, Y.-Q. Zhao, M.-Q. Cai, Theoretical study on photoelectric properties of lead-free mixed inorganic perovskite RbGe1-xSnxI3, Curr. Appl. Phys. 19 (2019) 279–284, <https://doi.org/10.1016/j.cap.2018.12.007>.
- [31] L. Gollino, T. Paupôtre, Lead-Less Halide Perovskite Solar Cells, Sol. RRL 5 (2021) 2000016, <https://doi.org/10.1002/solr.202000016>.
- [32] Y. Chen, Q. Meng, L. Zhang, C. Han, H. Gao, Y. Zhang, et al., SnO₂-based electron transporting layer materials for perovskite solar cells: A review of recent progress, J. Energy Chem. 35 (2019) 144–167, <https://doi.org/10.1016/j.jecchem.2018.11.011>.
- [33] A. Uddin, H. Yi, Progress and challenges of SnO₂ electron transport layer for perovskite solar cells: a critical review, Sol. RRL 6 (2022) 2100983, <https://doi.org/10.1002/solr.202100983>.
- [34] M.J. Paik, J.W. Yoo, J. Park, E. Noh, H. Kim, S.-G. Ji, et al., SnO₂-TiO₂ hybrid electron transport layer for efficient and flexible perovskite solar cells, ACS Energy Lett. 7 (2022) 1864–1870, <https://doi.org/10.1021/acsenergylett.2c00637>.
- [35] K. GangaReddy, M.V.R. Reddy, Physical vapour deposition of Zn²⁺ doped NiO nanostructured thin films for enhanced selective and sensitive ammonia sensing, Mater. Sci. Semicond. Process. 154 (2023) 107198, <https://doi.org/10.1016/j.mssp.2022.107198>.
- [36] N. Roy, Design and performance evaluation of MoS₂ photodetector in vertical MSM configuration, Opt. Mater. 148 (2024) 114817, <https://doi.org/10.1016/j.optmat.2023.114817>.
- [37] H.J. Snaith, M. Grätzel, Electron and Hole Transport through Mesoporous TiO₂ Infiltrated with Spiro-MeOTAD, Adv. Mater. 19 (2007) 3643–3647, <https://doi.org/10.1002/adma.200602085>.
- [38] Y. Peng, N. Yaacobi-Gross, A.K. Perumal, H.A. Faber, G. Vourlias, P.A. Patsalas, et al., Efficient organic solar cells using copper(I) iodide (CuI) hole transport layers, Appl. Phys. Lett. 106 (2015) 243302, <https://doi.org/10.1063/1.4922758>.
- [39] H.Y. Salah, M. Abdelfatah, A. El-Shaer, A.H. Oraby, Effect of Al doped ZnO on optical and photovoltaic properties of the p-Cu2O/n-AZO solar cells, Ceram. Int. 49 (2023) 7746–7752, <https://doi.org/10.1016/j.ceramint.2022.10.277>.
- [40] I. Suzuki, Z. Lin, T. Nogami, S. Kawanishi, B. Huang, A. Klein, et al., High open-circuit voltage in single-crystalline n-type SnS/MoO₃ photovoltaics, APL Mater. 11 (2023) 031116, <https://doi.org/10.1063/5.0143617>.
- [41] J. Song, M. Patel, S.E. Johannesson, K. Cho, J. Park, J. Kim, et al., Boosting wavelength-selective absorption and photocarrier collection in NiO/ZnO transparent photovoltaic heterojunctions by plasmonic Ag nanowire top

electrodes, *Adv. Electron. Mater.* 9 (2023) 2300326, <https://doi.org/10.1002/aelm.202300326>.

[42] J. Thiesbrummel, F. Peña-Camargo, K.O. Brinkmann, E. Gutierrez-Partida, F. Yang, J. Warby, et al., Understanding and minimizing VOC losses in all-perovskite tandem photovoltaics, *Adv. Energy Mater.* 13 (2023) 2202674, <https://doi.org/10.1002/aenm.202202674>.

[43] A. Kumar, S.K. Gupta, B.P. Dhamaniya, S.K. Pathak, S. Karak, Understanding the origin of defect states, their nature, and effects on metal halide perovskite solar cells, *Mater. Today Energy* 37 (2023) 101400, <https://doi.org/10.1016/j.mtener.2023.101400>.

[44] G. Li, Z. Su, L. Canil, D. Hughes, M.H. Aldamasy, J. Dagar, et al., Highly efficient p-i-n perovskite solar cells that endure temperature variations, *Science* 379 (2023) 399–403, <https://doi.org/10.1126/science.add7331>.

[45] G. Regmi, S. Rijal, S. Velumani, Unveiling the optimal selenization temperature for enhancing efficiency in flexible Cu(In, Ga)Se₂ thin film solar cells, *Curr. Appl. Phys.* 57 (2024) 49–58, <https://doi.org/10.1016/j.cap.2023.11.001>.

[46] M. Abdulmalik, E. Danladi, P. Boduku, J. Tasiu, M. Ahmad, N. Usman, Modeling and Simulation of Lead-Free Perovskite Solar Cell Using SCAPS-1D, *East Eur J Phys* 2021 (2021) 146–154, <https://doi.org/10.26565/2312-4334-2021-2-12>.

[47] M. Tripathi, V. Vaibhav Mishra, B.S. Sengar, A.V. Ullas, Lead-free perovskite solar cell by Using SCAPS-1D: Design and simulation, *Mater. Today: Proc.* 62 (2022) 4327–4331, <https://doi.org/10.1016/j.matpr.2022.04.832>.

[48] A.A. Goje, N.A. Ludin, M.A.M. Teridi, U. Syafiq, M.A. Ibrahim, F. Nawab, et al., Design and Simulation of Lead-free Flexible Perovskite Solar cell Using SCAPS-1D, *IOP Conf Ser Mater Sci Eng* 1278 (2023) 012004, <https://doi.org/10.1088/1757-899X/1278/1/012004>.

[49] A. Rmili, L. Soussi, R. Jdaa, T. Garmim, C. Louardi, A. El Bachiri, et al., Cu doped SnS thin films deposited by the spray method: characterization and numerical simulation using SCAPS-1D, *Opt. Quant. Electron.* 55 (2023) 424, <https://doi.org/10.1007/s11082-023-04665-4>.

[50] S. Moujoud, B. Hartiti, S. Touhtouh, C. Rachidy, F. Belhora, P. Thevenin, et al., Numerical modeling of copper indium disulfide thin film based solar cells, *Opt. Mater.* 122 (2021) 111749, <https://doi.org/10.1016/j.optmat.2021.111749>.

[51] S. Mehmood, Y. Xia, F. Qu, M. He, Investigating the Performance of Efficient and Stable Planer Perovskite Solar Cell with an Effective Inorganic Carrier Transport Layer Using SCAPS-1D Simulation, *Energies* 16 (2023) 7438, <https://doi.org/10.3390/en16217438>.

[52] Hasan Ali Md, Saiful Islam ATM, Haque MD, Ferdous Rahman Md, Khalid Hossain M, Sultana N, et al. Numerical analysis of FeSi₂ based solar cell with PEDOT:PSS hole transport layer. *Mater Today Commun* 2023;34:105387. Doi: 10.1016/j.mtcomm.2023.105387.

[53] S. Mathi, J. Sivapriya, M. Kalaiyari, J. Sivakumar, S.J. Rubavathy, A. Kumar, Analysing the performance ceiling of RbSnGeI₃-based lead-free stable perovskite solar cell, *Opt. Quant. Electron.* 55 (2023) 734, <https://doi.org/10.1007/s11082-023-04980-w>.

[54] G. Pindolia, S.M. Shinde, P.K. Jha, Optimization of an inorganic lead free RbGeI₃ based perovskite solar cell by SCAPS-1D simulation, *Sol. Energy* 236 (2022) 802–821, <https://doi.org/10.1016/j.solener.2022.03.053>.

[55] P.K. Jha, N.K. Chourasia, A. Srivastava, A.K. Sharma, R. Kumar, S. Sharma, et al., Study of Eco-Friendly Organic-Inorganic Heterostructure CH₃NH₃SnI₃ Perovskite Solar Cell via SCAPS Simulation, *J. Electron. Mater.* 52 (2023) 4321–4329, <https://doi.org/10.1007/s11664-023-10267-3>.

[56] Y. Zhang, X. Meng, X. Liu, F. Zhou, W. Yang, Y. Fan, et al., SCAPS simulation and DFT study of lead-free perovskite solar cells based on CsGeI₃, *Mater. Chem. Phys.* 306 (2023) 128084, <https://doi.org/10.1016/j.matchemphys.2023.128084>.

[57] M.K. Hossain, M.K.A. Mohammed, R. Pandey, A.A. Arnab, M.H.K. Rubel, K. M. Hossain, et al., Numerical Analysis in DFT and SCAPS-1D on the Influence of Different Charge Transport Layers of CsPbBr₃ Perovskite Solar Cells, *Energy Fuels* 37 (2023) 6078–6098, <https://doi.org/10.1021/acs.energyfuels.3c00353>.

[58] M. Abdelfatah, A.M. El Sayed, W. Ismail, S. Ulrich, V. Sitterer, A. El-Shaer, SCAPS simulation of novel inorganic ZrS₂/CuO heterojunction solar cells, *Sci. Rep.* 13 (2023) 4553, <https://doi.org/10.1038/s41598-023-31553-4>.

[59] M.D. Haque, M.H. Ali, M.F. Rahman, A.Z.M.T. Islam, Numerical analysis for the efficiency enhancement of MoS₂ solar cell: A simulation approach by SCAPS-1D, *Opt. Mater.* 131 (2022) 112678, <https://doi.org/10.1016/j.optmat.2022.112678>.

[60] U. Mandadapu, Performance analysis of NiO-based perovskite solar cell model, *Mater. Today: Proc.* (2023), <https://doi.org/10.1016/j.matpr.2023.03.025>.

[61] O. Mounkachi, E. Salmani, M. Lakhali, H. Ez-Zahraouy, M. Hamedoun, M. Benissa, et al., Band-gap engineering of SnO, *Sol. Energy Mater. Sol. Cells* 148 (2016) 34–38, <https://doi.org/10.1016/j.solmat.2015.09.062>.

[62] D. Ompong, M. Clements, Optimization of formamidinium-based perovskite solar cell using SCAPS-1D, *Results Opt.* 14 (2024) 100611, <https://doi.org/10.1016/j.rio.2024.100611>.

[63] H. Bencherif, F. Meddour, M.H. Elshorbagy, M. Khalid Hossain, A. Cuadrado, M. A. Abdi, et al., Performance enhancement of (FAPbI₃)_{1-x}(MAPbBr₃)_x perovskite solar cell with an optimized design, *Micro Nanostructures* 171 (2022) 207403, <https://doi.org/10.1016/j.micrna.2022.207403>.

[64] F. Kherrat, L. Dehimi, H. Bencherif, M.M.A. Moon, M.K. Hossain, N.A. Sonmez, et al., Performance enhancement of eco-friendly Cs₃Sb₂I₉-based perovskite solar cell employing Nb₂O₅ and CuI as efficient charge transport layers, *Micro Nanostruct.* 183 (2023) 207676, <https://doi.org/10.1016/j.micrna.2023.207676>.

[65] M. Rai, L.H. Wong, L. Etgar, Effect of Perovskite Thickness on Electroluminescence and Solar Cell Conversion Efficiency, *J. Phys. Chem. Lett.* 11 (2020) 8189–8194, <https://doi.org/10.1021/acs.jpclett.0c02363>.

[66] C. Momblona, O. Malinkiewicz, C. Roldán-Carmona, A. Soriano, L. Gil-Escrí, E. Bandiello, et al., Efficient methylammonium lead iodide perovskite solar cells with active layers from 300 to 900 nm, *APL Mater.* 2 (2014) 081504, <https://doi.org/10.1063/1.4890056>.

[67] J. Madan, K. Singh, R. Pandey, Comprehensive device simulation of 23.36% efficient two-terminal perovskite-PbS CQD tandem solar cell for low-cost applications, *Sci. Rep.* 11 (2021) 19829, <https://doi.org/10.1038/s41598-021-99098-y>.

[68] A. Mortadi, E. El Hafidi, M. Monkade, R. El Moznine, Investigating the influence of absorber layer thickness on the performance of perovskite solar cells: A combined simulation and impedance spectroscopy study, *Mater. Sci. Energy Technol.* 7 (2024) 158–165, <https://doi.org/10.1016/j.mset.2023.10.001>.

[69] U.C. Obi, D.M. Sanni, A. Bello, Effect of Absorber Layer Thickness on the Performance of Bismuth-Based Perovskite Solar Cells, *Semiconductors* 55 (2021) 922–927, <https://doi.org/10.1134/S1063782621040114>.

[70] N. Shrivastav, J. Madan, R. Pandey, Predicting photovoltaic efficiency in Cs-based perovskite solar cells: a comprehensive study integrating SCAPS simulation and machine learning models, *Solid State Commun.* 380 (2024) 115437, <https://doi.org/10.1016/j.ssc.2024.115437>.

[71] S.R. Hosseini, M. Bahramgour, P. Yardani Sefidi, A. Tabatabaei Mashayekh, A. Moradi, N. Delibas, et al., Investigating the effect of non-ideal conditions on the performance of a planar CH₃NH₃PbI₃-based perovskite solar cell through SCAPS-1D simulation, *Helyon* 8 (2022) e11471.

[72] K. Bakker, A. Rasia, S. Assen, B.B.S. Aflouat, A. Weeber, M. Theelen, How the absorber thickness influences the formation of reverse bias induced defects in CIGS solar cells, *EPJ Photovolt* 11 (2020) 9, <https://doi.org/10.1051/epjpv/2020006>.

[73] C. Wang, J. Wu, X. Liu, S. Wang, Z. Yan, L. Chen, et al., High-effective SnO₂-based perovskite solar cells by multifunctional molecular additive engineering, *J. Alloy. Compd.* 886 (2021) 161352, <https://doi.org/10.1016/j.jallcom.2021.161352>.

[74] M.K. Hossain, G.F.I. Toki, A. Kuddus, M.H.K. Rubel, M.M. Hossain, H. Bencherif, et al., An extensive study on multiple ETL and HTL layers to design and simulation of high-performance lead-free CsSnCl₃-based perovskite solar cells, *Sci. Rep.* 13 (2023) 2521, <https://doi.org/10.1038/s41598-023-28506-2>.

[75] T.S. Sherkar, C. Momblona, L. Gil-Escrí, J. Ávila, M. Sessolo, H.J. Bolink, et al., Recombination in perovskite solar cells: significance of grain boundaries, interface traps, and defect ions, *ACS Energy Lett.* 2 (2017) 1214–1222, <https://doi.org/10.1021/acsenergylett.7b00236>.

[76] R. Lin, K. Xiao, Z. Qin, Q. Han, C. Zhang, M. Wei, et al., Monolithic all-perovskite tandem solar cells with 24.8% efficiency exploiting co-proportionation to suppress Sn(II) oxidation in precursor ink, *Nat. Energy* 4 (2019) 864–873, <https://doi.org/10.1038/s41560-019-0466-3>.

[77] L. Xiong, M. Qin, G. Yang, Y. Guo, H. Lei, Q. Liu, et al., Performance enhancement of high temperature SnO₂-based planar perovskite solar cells: electrical characterization and understanding of the mechanism, *J. Mater. Chem. A* 4 (2016) 8374–8383, <https://doi.org/10.1039/C6TA01839D>.

[78] V.P. Hoang Huy, T.M.H. Nguyen, C.W. Bark, Recent Advances of Doped SnO₂ as Electron Transport Layer for High-Performance Perovskite Solar Cells, *Materials* 16 (2023) 6170, <https://doi.org/10.3390/ma16186170>.

[79] H. Yang, Y. Shen, G. Xu, F. Yang, X. Wu, J. Ding, et al., Functional Spiro-OMeTAD-like dopant for Li-Ion-free hole transport layer to develop stable and efficient n-i-p perovskite solar cells, *Nano Energy* 119 (2024) 109033, <https://doi.org/10.1016/j.nanoen.2023.109033>.

[80] A. Bag, R. Radhakrishnan, R. Nekovei, R. Jeyakumar, Effect of absorber layer, hole transport layer thicknesses, and its doping density on the performance of perovskite solar cells by device simulation, *Sol. Energy* 196 (2020) 177–182, <https://doi.org/10.1016/j.solener.2019.12.014>.

[81] J.J. Do, J.R. Kwon, D. Kim, J.W. Jung, Minimized defective trap sites in perovskite absorber films by coumarin dye for efficient and reliable perovskite solar cells, *Dyes Pigm.* 221 (2024) 111831, <https://doi.org/10.1016/j.dyepig.2023.111831>.

[82] M.S. Jamal, S.A. Shahahmadi, A.W. MohdA, P. Chelvanathan, N. Asim, H. Misran, et al., Effect of defect density and energy level mismatch on the performance of perovskite solar cells by numerical simulation, *Optik* 182 (2019) 1204–1210, <https://doi.org/10.1016/j.jle.2018.12.163>.

[83] A.S. Chouhan, N.P. Jasti, S. Avasthi, Effect of interface defect density on performance of perovskite solar cell: Correlation of simulation and experiment, *Mater. Lett.* 221 (2018) 150–153, <https://doi.org/10.1016/j.matlett.2018.03.095>.

[84] E.O. Shalenov, Y.S. Seitkozhanov, C. Valagiannopoulos, A. Ng, K. N. Dzhumagulova, A.N. Jumabekov, Performance evaluation of different designs of back-contact perovskite solar cells, *Sol. Energy Mater. Sol. Cells* 234 (2022) 111426, <https://doi.org/10.1016/j.solmat.2021.111426>.

[85] S. Ghosh, S. Porwal, T. Singh, Investigation of the role of back contact work function for hole transporting layer free perovskite solar cells applications, *Optik* 256 (2022) 168749, <https://doi.org/10.1016/j.jle.2022.168749>.

[86] A.K. Das, R. Mandal, D.K. Mandal, Impact of HTM on lead-free perovskite solar cell with high efficiency, *Opt. Quant. Electron.* 54 (2022) 455, <https://doi.org/10.1007/s11082-022-03852-z>.

[87] S.S. Bal, A. Basak, U.P. Singh, Numerical modeling and performance analysis of Sb-based tandem solar cell structure using SCAPS – 1D, *Opt. Mater.* 127 (2022) 112282, <https://doi.org/10.1016/j.optmat.2022.112282>.

[88] Q. Meng, Y. Chen, Y.Y. Xiao, J. Sun, X. Zhang, C.B. Han, et al., Effect of temperature on the performance of perovskite solar cells, *J. Mater. Sci. Mater. Electron.* 32 (2021) 12784–12792, <https://doi.org/10.1007/s10854-020-03029-y>.

[89] E. Aktas, N. Rajamanickam, J. Pascual, S. Hu, M.H. Aldamasy, D. Di Girolamo, et al., Challenges and strategies toward long-term stability of lead-free tin-based

perovskite solar cells, *Commun. Mater.* 3 (2022) 1–14, <https://doi.org/10.1038/s43246-022-00327-2>.

[90] A. Dilawar Khan, M. Mustajab, S. Moeen, M. Imran, M. Ikram, Q. Khan, et al., Advancements in the stability, protection and lead-free strategies of perovskite solar cells: a critical review, *Environ. Sci. Adv.* 3 (2024) 1004–1029, <https://doi.org/10.1039/D3VA00401E>.

[91] H.A. Reshi, R.A. Zargar, H.A. Reshi, R.A. Zargar, perovskite solar cells: the challenging issues for stable power conversion efficiency, *Recent Dev. Optoelectron. Devices*, IntechOpen (2018), <https://doi.org/10.5772/intechopen.75406>.